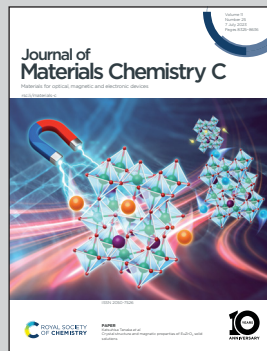


Showcasing research from Zhejiang Sci-Tech University,  
Hangzhou, China

A highly stretchable and sensitive strain sensor for  
lip-reading extraction and speech recognition

A CuNWs-rGO/PDMS strain sensor translates lip movements directly into speech or text by capturing lip muscle movements. It presents a promising way to help people with vocal cord lesions or laryngeal and speech impairments to communicate without barriers and will enrich the diversity of lip-reading systems in human-machine and silent speech interfaces.

As featured in:



See Lin Cheng *et al.*,  
*J. Mater. Chem. C*, 2023, **11**, 8542.



Cite this: *J. Mater. Chem. C*, 2023,  
11, 8413

## A highly stretchable and sensitive strain sensor for lip-reading extraction and speech recognition†

Lin Cheng, <sup>a</sup> Diqing Ruan, <sup>a</sup> Yongwei He, <sup>a</sup> Jiayao Yang, <sup>a</sup> Wei Qian, <sup>a</sup> Longwei Zhu, <sup>b</sup> Pindie Zhu, <sup>b</sup> Huaping Wu \*<sup>c</sup> and Aiping Liu \*<sup>a</sup>

Speech recognition often relies on visual stereo images and videos, but it is often limited by light intensity and opaque occlusions such as masks (such as during the coronavirus disease 2019 (COVID-19) pandemic). Lip speech is produced by the movement of a series of muscles in the mouth. Therefore, lip-reading extraction and decoding can be achieved by attaching non-invasive sensors to capture muscle movement. Herein, we prepared a highly sensitive and stretchable CuNW-rGO/PDMS piezoresistive strain sensor based on a biomimetic pearl "brick-mortar" structure by using two-dimensional rGO and conductive stretchable one-dimensional Cu NWs as mixed "bricks" and stretchable PDMS as the "mortar". The strain sensor shows a high sensitivity with a gauge factor of 26 in the stretching ability range of up to 70% and high durability over 1000 stretching-releasing cycles. This sensor can act as a health monitoring device when attached to human skin, detecting various human motions such as hand clenching, elbow bending, wrist pulse beating and lip-reading motion. Effective recognition of the lip reading signal was achieved by processing the lip-reading signal using a dynamic time regularization algorithm and Euclidean distance. Finally, a full system integration to real-time analyze and feedback speech information with voice broadcast and text display function based on the strain sensor was presented for accurate speech recognition, which opens up a new possibility for translating lip motion to speech or text directly by capturing lip muscle movements. This work presents a promising way to help people with vocal cord lesions or laryngeal and lingual injuries live a happy life with barrier-free communication and will enrich the diversity of lip-language translation systems in human-machine interfaces and silent speech interfaces.

Received 31st March 2023,  
Accepted 15th May 2023

DOI: 10.1039/d3tc01136d

rsc.li/materials-c

### Introduction

Speech recognition usually depends on visual stereo images and videos to record and identify visible movement of speech articulators such as vocal cords, lips, facial muscles and the tongue in a nonintrusive manner.<sup>1–5</sup> Comprehensive analysis of visual features is further necessary by multiple signal processing techniques including motion segmentation, wavelet transform and complicated computation.<sup>6,7</sup> However, the accurate extraction of these static and motion features relies on the geometric shape of speech articulators and the pixel intensity of the images

by using an expensive instrument or high-definition camera, and might be influenced by the facial angles, light intensity, head shaking and blocking objects, thus hampering their communication in a natural and flexible manner.<sup>8</sup> Moreover, when a speaker's mouth is covered by an opaque mask, as is the case in an epidemic of respiratory infectious diseases (currently, the coronavirus disease 2019 (COVID-19) pandemic), the speech recognition of vision-based solutions fails.

Recently, wearable electronic devices have emerged as a promising technology that can be worn or conformally attached to human skin to monitor an individual's activities in real time and continuously, without interfering with or restricting the user's motions, thus providing more accurate and reliable quantitative analysis.<sup>9–13</sup> Many high-performance (high sensitivity and selectivity) flexible strain sensors have been reported, such as graphene-based flexible sensors, conducting hydrogel-based flexible sensors, and fiber-based smart sensors.<sup>14–20</sup> However, most wearable strain sensors are capable of tracking individual speech information through the vocal cord vibration of the speaker.<sup>21–25</sup> For instance, Gao *et al.*<sup>22</sup> fabricated a strain sensor based on fragmented carbonized melamine sponges and attached the strain sensor to the epidermis 2 cm below the throat of the tester to record the specific changes in the

<sup>a</sup> Key Laboratory of Optical Field Manipulation of Zhejiang Province, School of Materials Science & Engineering, Zhejiang Sci-Tech University, Hangzhou 310018, China. E-mail: liuaiping1979@gmail.com

<sup>b</sup> School of Information Science & Technology, Zhejiang Sci-Tech University, Hangzhou 310018, China

<sup>c</sup> Key Laboratory of Special Purpose Equipment and Advanced Processing Technology, Ministry of Education and Zhejiang Province, College of Mechanical Engineering, Zhejiang University of Technology, Hangzhou 310023, China. E-mail: wuhaping@gmail.com

† Electronic supplementary information (ESI) available. See DOI: <https://doi.org/10.1039/d3tc01136d>

electrical signal when the tester read the letters “E”, “C”, “U”, “S” and “T”, which showed excellent pronunciation recognition ability. Yan *et al.*<sup>23</sup> presented a two-stage solvothermal freeze-casting approach to fabricate an all carbon aerogel (MGA) with a multi-arched structure, indicating excellent reproducibility, timely wireless communication, and stability when attached to the volunteer’s throat and reading different languages (Chinese, English, and Russian). Tao *et al.*<sup>24</sup> developed a wearable and low-cost artificial throat with good performance in generating and detecting sounds when it was attached to the throat. But the artificial throat may not be suitable for people with vocal cord damage who retain the ability to speak but lose the capacity to phonate *via* vocal cords, and the speech recognition and decoding system *via* the wearable sensor has not been explored.<sup>25</sup>

Lip language is produced by the movement of a series of muscles in the mouth. Non-invasive, contact sensors that capture muscle movement are not affected by visual recognition and provide an effective way to obtain valid language information from muscle movements.<sup>26,27</sup> Inspired by nature, the structural design of natural nacre, which features an “inorganic brick–organic mortar” structure, can be extended to sensing materials, allowing the prepared sensor to achieve a high gauge factor and a wide sensing range simultaneously.<sup>28,29</sup> PDMS demonstrates good biocompatibility and tensile properties, making it suitable for “organic mortar”.<sup>30</sup> Two-dimensional (2D) graphene nanosheets, which possess extraordinary electrical and mechanical properties, are ideal candidates for “inorganic bricks”. However, graphene oxide (GO) sheets tend to restack due to  $\pi$ - $\pi$  stacking during the reduction.<sup>31</sup> One-dimensional (1D) metal nanowires can be intercalated between the GO sheets to inhibit the stacking of rGO, facilitating the slippage of rGO and also providing another electron transport path.<sup>32</sup> Copper nanowires (Cu NWs) are considered promising alternatives to Ag NWs or Au NWs due to their comparable electrical and thermal conductivity, high abundance (1000 times more abundant than silver) and low cost (100 times less expensive than silver).<sup>33</sup>

Considering the sensitivity, sensing range and the above characteristics of sensing nanomaterials, we prepared a highly sensitive and stretchable CuNW-rGO/PDMS piezoresistive strain sensor based on a biomimetic pearl “brick-mortar” structure by using 2D rGO and conductive stretchable 1D Cu NWs as mixed “bricks” and stretchable PDMS as the “mortar”. As a proof of concept, the CuNW-rGO/PDMS strain sensor can be employed as a health monitoring device to detect various human motions. In addition, when connected to the lips, it shows a unique recognition of lip muscle movements. Converting the lip muscle movement signals captured by the sensor into speech or text provides an effective way for individuals with language barriers to enjoy barrier-free communication and enhances the diversity of lip language translation systems in the human-computer interface and silent speech interface.

## Experimental section

### Materials

Graphite flake (325 mesh) was provided by Alfa Aesar Co. Ltd. (Shanghai, China). All the chemical reagents for the oxidation of graphite, such as concentrated sulfuric acid ( $H_2SO_4$ , 98%),

potassium permanganate ( $KMnO_4$ ), sodium nitrate ( $NaNO_3$ ), and hydrogen peroxide solution ( $H_2O_2$ ), were of analytical grade and purchased from Tianjin Hengxing Chemical Reagent Manufacturing Co., Ltd. Ethylenediamine (EDA, 99.0) was obtained from Sinopharm Chemical Reagent Co., Ltd. (Shanghai, China). Hydrazine solution ( $N_2H_4$ , 80% in  $H_2O$ ) and L-ascorbic acid ( $C_6H_8O_6$ , 99.99%) were obtained from Macklin (Shanghai, China). Sodium hydroxide ( $NaOH$ , 99.0%) was purchased from Inner Mongolia Junzheng Energy & Chemical Group Co., Ltd. (Inner Mongolia, China). Anhydrous ethanol (99%) was obtained from Greagent Co., Ltd. Ethylene glycol was obtained from Macklin (Shanghai, China). All reagents were of analytical grade and used as received without further purification. For all experiments involving human subjects, informed consent was obtained.

### Synthesis of graphene oxide

Graphene oxide (GO) was fabricated according to the modified Hummers’ method.<sup>34</sup> Typically, graphite (1 g) and  $NaNO_3$  (0.5 g) were stirred with dropping  $H_2SO_4$  (25 mL) slowly. Then  $KMnO_4$  was added and reacted in an ice-water bath for 1 h and then transferred to a 35–37 °C water bath for another 1 h. After  $H_2O_2$  solution was added into the mixture to terminate the reaction, the color of the mixture became bright yellow. Finally, the bright yellow solution was centrifuged and washed to obtain the GO solution. The prepared GO solution was freeze-dried to facilitate further calibration of the GO concentration.

### Synthesis of CuNWs

The CuNWs were prepared according to the method reported by Ye *et al.*<sup>35</sup> Briefly, 15 M  $NaOH$  solution (20 mL) was taken in a round-bottomed flask at 60 °C, then 1 mL  $Cu(NO_3)_2$  was dropped into the  $NaOH$  solution slowly. After 15 min, 170  $\mu$ L ethylenediamine and 30  $\mu$ L  $N_2H_4$  (35 wt%) were added into the mixture at 60 °C for 90 min. After the mixture was transferred to an ice-water bath for 10 min, the CuNWs were obtained after centrifugation.

### Fabrication of a CuNW-rGO/PDMS strain sensor

The schematic of the fabrication process of the CuNW-rGO/PDMS strain sensor is shown in Fig. 1. Firstly, 5 mg CuNW ethanol solution was dispersed in 22 mL ethylene glycol under magnetic stirring. Then 50 mg ascorbic acid and 3 mL GO solution (8 mg  $mL^{-1}$ ) were added to the CuNW ethanol solution and reacted at 120 °C for 4 h in a hydrothermal reactor to obtain the CuNW-rGO hydrogel. After the CuNW-rGO hydrogel was washed repeatedly and fragmentized by magnetic stirring, the mixture was filtered to form the CuNW-rGO film with a three-dimensional porous structure. Subsequently, the CuNW-rGO film was freeze-dried and cut into strips (2 cm × 0.5 cm) or designed shapes. Then liquid PDMS (Sylgard 184, Dow Corning) was poured onto the film and infiltrated the porous structure of CuNW-rGO film with large amounts of bubbles removed in a vacuum chamber. Finally, the strain sensor was fabricated by curing the CuNW-rGO/PDMS at 70 °C.

### Characterization

The morphologies of the CuNW, CuNW-rGO and CuNW-rGO/PDMS samples were investigated using a field emission

scanning electron microscope (FE-SEM, Hitachi S4800). The crystalline structure of CuNW-rGO was investigated using an X-ray diffractometer (Bruker AXS D8) using the Cu K $\alpha$  radiation ( $\lambda = 0.15418$  nm) with the  $2\theta$  scan from  $10^\circ$  to  $90^\circ$  at a step of  $0.02^\circ$ . The structure analysis of GO and CuNW-rGO was performed using a Raman spectrometer (Thermo Fisher DXR) equipped with an objective ( $50\times$ ) using a He-Ne laser ( $\lambda = 632.8$  nm). Resistance characteristics of the strain sensor and resistance changes during stretching were measured using a source meter (Keithley 2400). The real-time tests of the electromechanical properties of the strain sensor were carried out by using a Keithley 4200 source meter with a two-probe measurement system.

## Results and discussion

### Design of a CuNW-rGO/PDMS composite strain sensor

The schematic illustration of the fabrication process of a CuNW-rGO/PDMS strain sensor is illustrated in Fig. 1. The CuNWs and GO were first mixed with ascorbic acid to form a hydrogel under hydrothermal conditions. The hydrogel was fragmentized into pieces in deionized water and vacuum-filtrated to form a CuNW-rGO film. Then the CuNW-rGO film was peeled off from the filter paper and cut into desired shapes (such as rectangular or V-shaped strips). After “mortar” PDMS was poured in and cured, the CuNW-rGO/PDMS composite strain sensor with Cu wire connection was obtained. The “brick-mortar” structure sensor can be used to monitor various strains such as stretching, compressing, bending and twisting as well as human motions.

### Morphology and structure of the CuNW-rGO/PDMS composite strain sensor

Fig. 2(a) shows the photograph and scanning electron microscopy (SEM) image of the CuNW-rGO film with a porous structure, which can help withstand greater strain. The CuNWs (with  $50\text{--}60$   $\mu\text{m}$  in length and  $200\text{--}300$  nm in diameter, see Fig. S1 in the ESI<sup>†</sup>) are evenly distributed in the rGO pieces (Fig. 2b). From the cross-sectional SEM images in Fig. 2(c) and (d), the multi-layered and porous structure of the CuNW-rGO hybrid with  $200$   $\mu\text{m}$  thickness is clearly observed, and the structure remains very well after the “organic mortar” PDMS is infiltrated into the “inorganic brick” with porous structure CuNW-rGO

(Fig. 2e and f). The structure of the CuNW-rGO hybrid was further investigated by the X-ray diffraction (XRD) and Raman measurements (Fig. 2g and h). The apparent diffraction peak of (002) at  $11.2^\circ$  for GO moves to  $24.5^\circ$ , indicating the successful reduction from GO to rGO after the hydrothermal reaction.<sup>36</sup> The three strong diffraction peaks at  $43.3^\circ$ ,  $50.4^\circ$  and  $74.1^\circ$  can be assigned to the (111), (200) and (220) crystalline planes of face-centered cubic Cu (JCPDS 04-0836), respectively. From the Raman spectra, GO and rGO display two prominent peaks at around  $1345$   $\text{cm}^{-1}$  (D band) and  $1580$   $\text{cm}^{-1}$  (G band).<sup>37</sup> The intensity ratio of the D-band and G-band ( $I_D/I_G$ ) increases from 0.93 for GO to 1.10 for CuNW-rGO, suggesting partial restoring of the conjugation structure during the reduction process of GO. Additionally, Fig. 2i shows the current–voltage ( $C$ – $V$ ) curve of the rGO/PDMS and CuNW-rGO/PDMS. With the addition of CuNWs, the conduction paths of flexible sensors increase, and the conduction mode of the original single “surface-to-surface” contact of the rGO sheet has changed to the “face-to-face” contact of the rGO sheet, “line-to-line” contact between CuNWs and the “line-to-face” contact between rGO and CuNWs, thus the addition of CuNWs is very important in keeping and increasing the conductivity of the CuNW-rGO/PDMS sensor and improving the sensitivity of the strain sensor by withstanding greater strains.

### Electrical performance of the CuNW-rGO/PDMS composite strain sensor

Fig. 3(a) reveals the change of relative resistance along with strains from 0 to 70% and the slope of the curve is defined as the gauge factor  $G = (\Delta R/R)/\varepsilon$ , where  $\Delta R$ ,  $R$  and  $\varepsilon$  represent the change of resistance, original resistance without strains, and the ratio of elongation, respectively.<sup>38</sup> As the strain increases, the hexagonal honeycomb-like sheet structure of rGO is first elongated and then local cracks are generated, resulting in an increase in the distance between the continuous CuNW-rGO sheets and a decrease in the contact area as well as the conduction path (Fig. 3j).<sup>39–41</sup> When the strain is removed, the rGO sheets at the crack are re-stacked or re-connected through CuNWs due to the viscoelasticity of PDMS, so that the conductivity of the CuNW-rGO/PDMS porous composite film can basically be restored to the original state. The high gauge factor of about 26 is attributed to the porous structure of rGO and infiltration of “mortar” PDMS as well as the addition

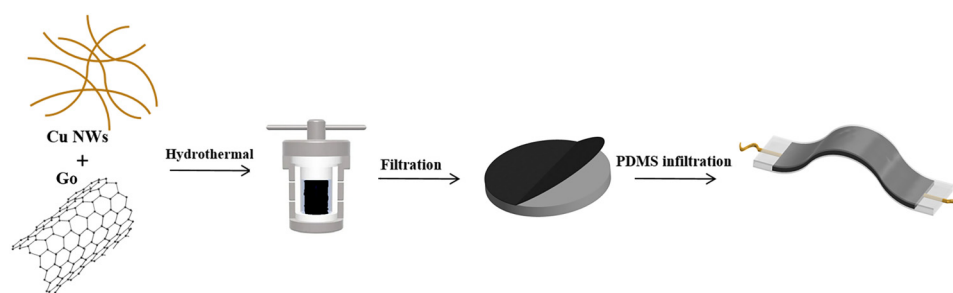
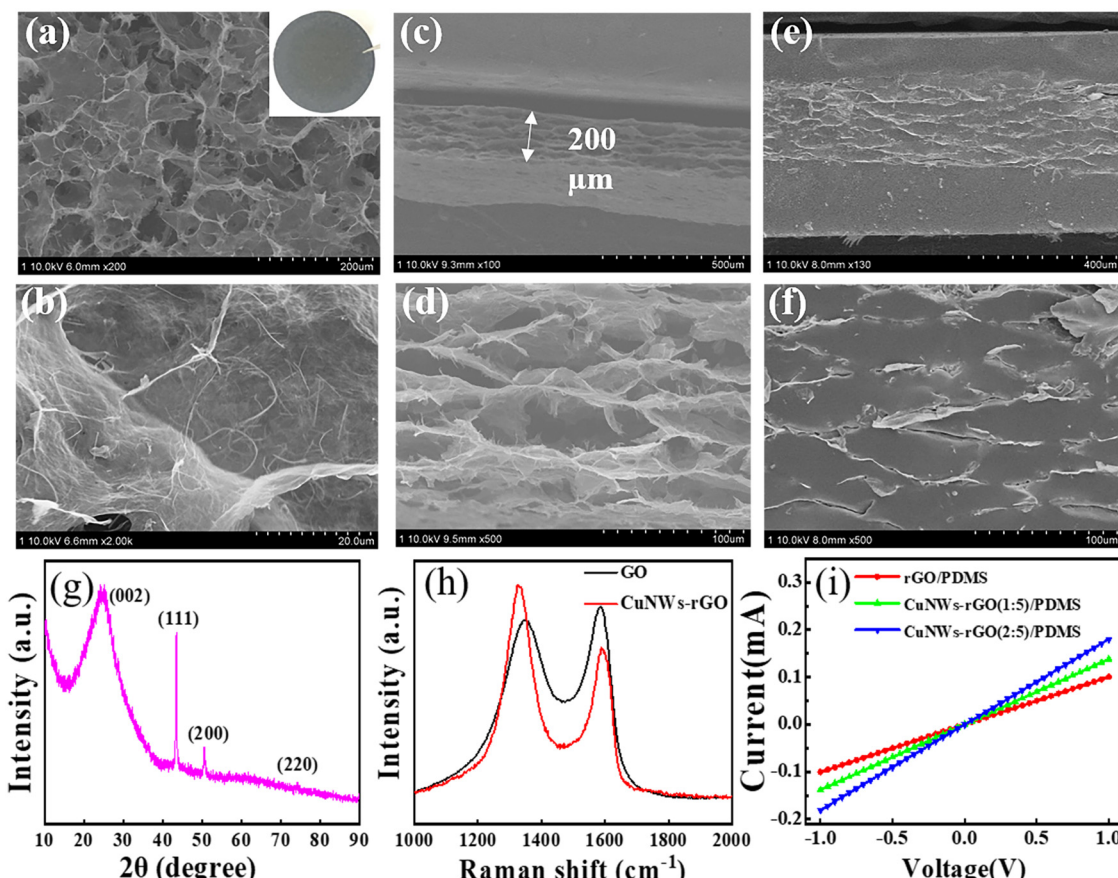


Fig. 1 The schematic illustration of the fabrication process of a CuNW-rGO/PDMS strain sensor.



**Fig. 2** Basic characterization of the stretchable and flexible CuNW-rGO/PDMS hybrid film. (a) and (b) Top view SEM images of CuNW-rGO with a porous structure and exposed CuNWs. (c) and (d) Cross-sectional views showing the multi-layered and porous structure of the CuNW-rGO film with 200  $\mu\text{m}$  thickness. (e) and (f) Cross-sectional view SEM images of the CuNW-rGO/PDMS strain sensor with "mortar" PDMS infiltrated into the porous structure of "brick" CuNW-rGO. (g) X-ray diffraction (XRD) pattern of the CuNW-rGO film. (h) Raman spectra of the GO and CuNW-rGO film. (i) The conductivity of rGO/PDMS and CuNW-rGO/PDMS samples with different mass ratios of CuNW-GO.

of CuNWs to improve the conductivity and conductive path of the strain sensor in the tensile process. However, increasing the amount of CuNWs allows the sensor to detect up to 70% change in tensile strain, albeit with a decreased sensitivity from 26 to 13.4 (Fig. S2a, ESI<sup>†</sup>). This is due to the tendency of the excess CuNWs to accumulate in the rGO layer and to be unevenly distributed (Fig. S2b, ESI<sup>†</sup>). Although this process enhances the conductivity of the sensor (Fig. 2i), it also negatively affects the mechanical properties and sensitivity of the sensor. Therefore, a high-sensitivity strain sensor with a suitable ratio of CuNW-rGO was used for subsequent experiments. Fig. 3b shows the frequency independence of the flexible strain sensor under a constant strain of 30%. Under the same tensile strain, a repeatability test of 1000 loading and unloading cycles proved the excellent repeatability and stability (Fig. 3c). The response and relaxation times are very short (Fig. 3f) due to the sensitive materials of CuNWs and rGO and the viscoelastic behavior of PDMS. Fig. 3d and e demonstrate that the strain sensor also exhibits a satisfactory linearity of the electrical signal in different bending and twisting states. In addition, the sensor demonstrates good repeatability and stability for complex mechanical stimuli such as twisting while

stretching (Fig. 3g), twisting in both directions (Fig. 3h), and twisting in one direction (Fig. 3i).

#### Human bodily motion detection *via* the CuNW-rGO/PDMS composite strain sensor

Human motion monitoring was carried out by using the CuNW-rGO/PDMS composite strain sensor. As shown in Fig. 4(a and b), the sensor can tightly attach to human skin by using a medical tape, which can monitor the electrical signal when making a fist and elbow movement, presenting different processes of muscle motion with fast response and high sensitivity. The large increase in the resistance signal is due to the cracks produced between the CuNW-rGO layers during the muscle stretching process, which reduces the contact area and conductive path. The results indicate that the sensor is suitable for large strain detection and can be used as a wearable device for health monitoring and medical examination. In addition, the CuNW-rGO/PDMS hybrid film can detect less than 1% strain such as a wrist pulse with three characteristic peaks (Fig. 4c), thus has potential application prospects in the field of smart medical care.

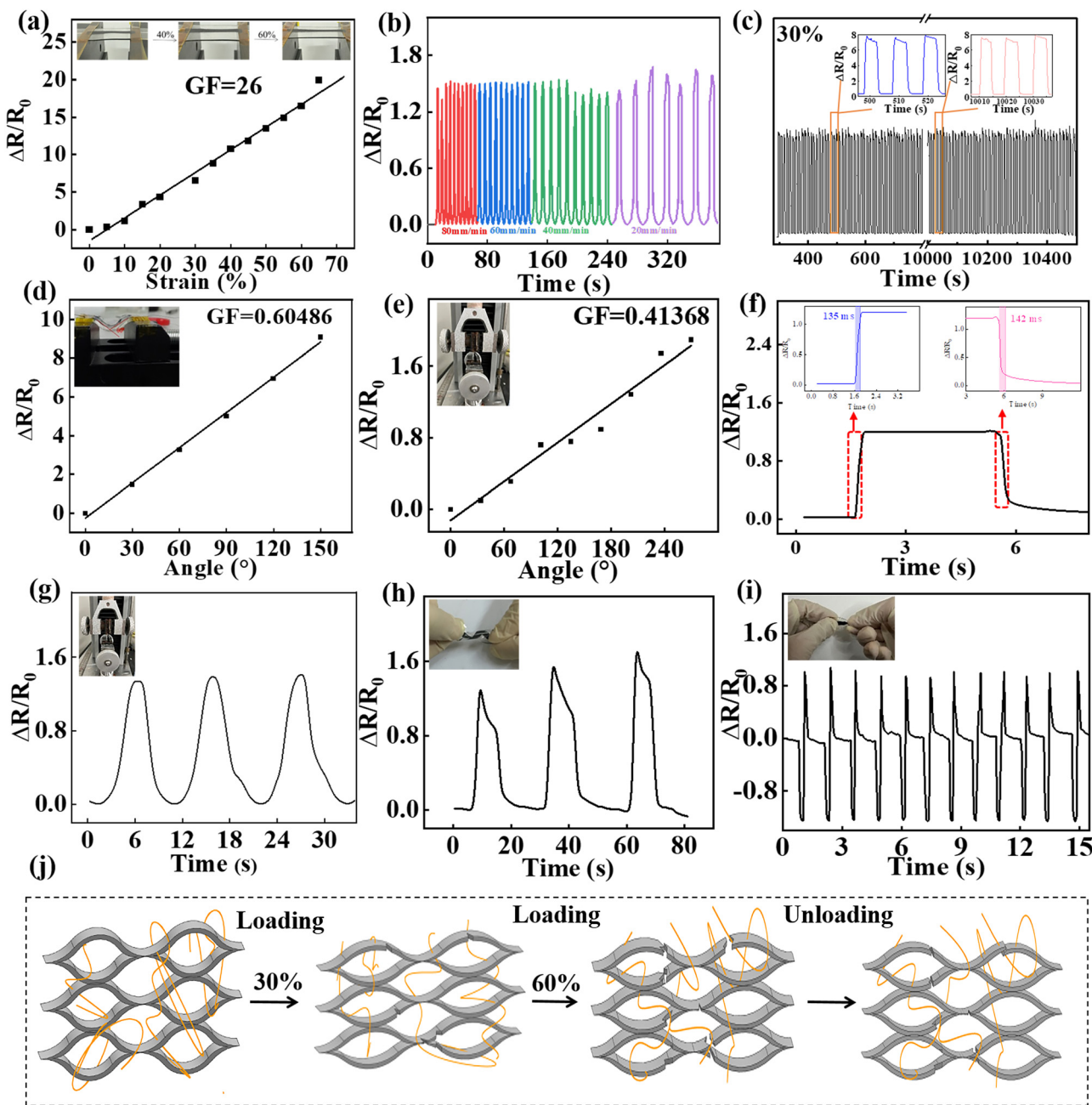


**Fig. 3** (a) The change of relative resistance along with strains and the slope showing the gauge factor of the strain sensor. The inset shows the optical images of the sensor during stretching. (b) Frequency independence under a constant strain of 30%. (c) Repeatable experiment over 1000 cycles of 30% loading–unloading process. Insets show partially enlarged views. (d) The relative resistance changes under different bending angles. The inset shows the optical image of the bending test. (e) Twisting test under different angles. The inset shows the optical image of the twisting test. (f) Response and recovery time measurements. (g) The repeatable test of twisting, while stretching. (h) The repeatable test of twisting in both directions. (i) The repeatable test of twisting in one direction. The inset in the g–i show the optical images corresponding to the test procedure. (j) The sensing mechanism of CuNW-rGO/PDMS sensors under strains.

### Lip-reading detection and speech recognition application of the CuNW-rGO/PDMS composite strain sensor

Currently, deaf-mute people have great obstacles in communicating with normal people, which causes inconvenience in life and communication for deaf-mute people. Sign language solves this problem, but it is very limited for most normal people who do not understand sign language. Additionally,

many dumb people who are unable to speak due to damage to their vocal cords have not learned sign language systematically, so find it difficult to communicate with people. The current lip language recognition technology uses camera shooting and image processing methods to extract the characteristics of the lip image to recognize lip language.<sup>42–45</sup> This method is not only difficult to implement, it also has cumbersome operating

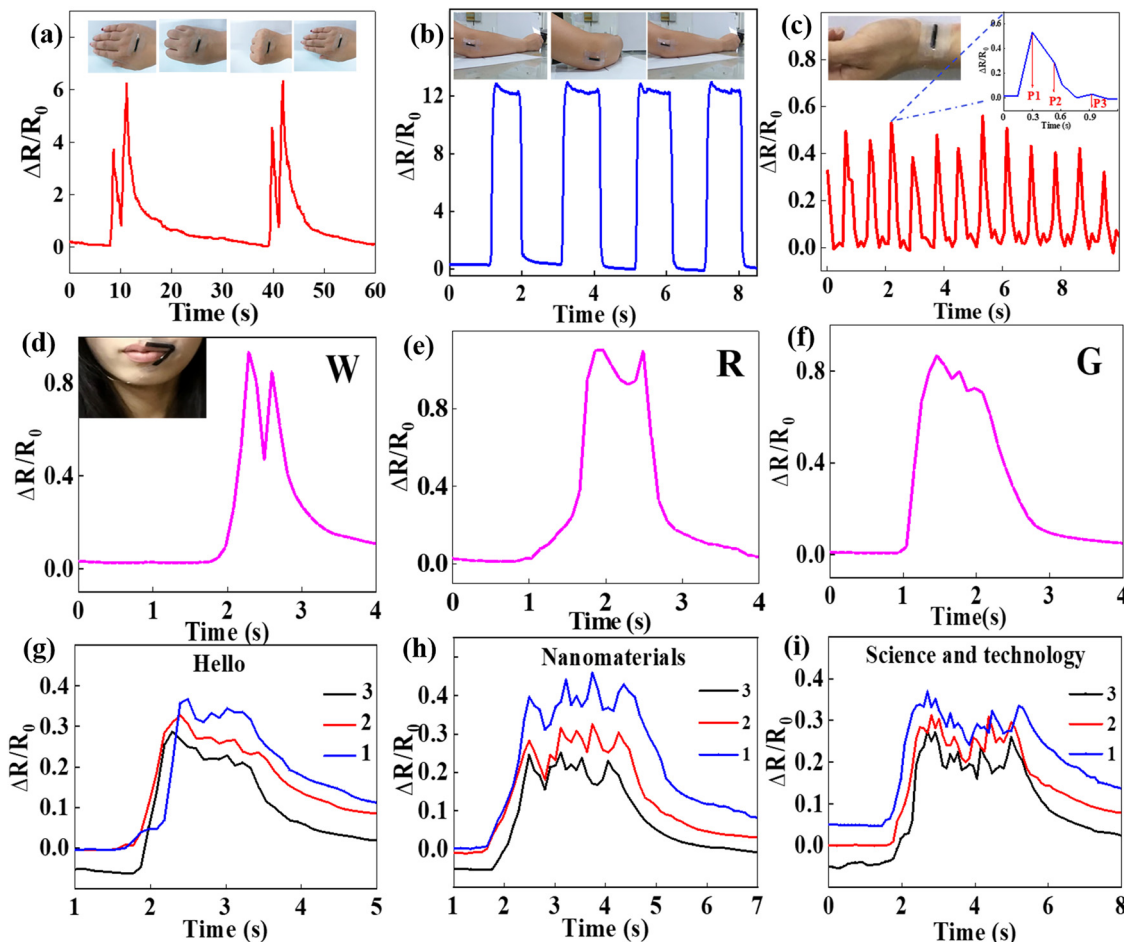


**Fig. 4** Human bodily motion detection of the CuNW-rGO/PDMS composite strain sensor. (a) and (b) Relative resistance changes of fist and elbow bending, respectively. Corresponding inset figures represent the human motion processes. (c) Relative resistance change and corresponding optical picture of a wrist pulse beating test. Inset shows the relative resistance change of one wrist pulse beat. (d–f) The relative resistance changes of the sensor when reading letters “W”, “R”, and “G”. The inset image represents the optical photograph of a volunteer wearing the sensor around the lip. (g–i) The relative resistance change of the sensor when reading “hello”, “nanomaterials” and “science and technology”.

steps, and is of high cost, which is not conducive to large-scale industrialization. Therefore, we have done a meaningful test in lip-reading signal acquisition, recognition and auxiliary pronunciation. When an arcuate CuNW-rGO/PDMS sensor is attached to the orbicularis muscle around the lip with medical tape (inset of Fig. 4d), we can collect the movement of the muscles around the lips when reading 26 English letters and some commonly used words (“hello”, “nanomaterials” and “science and technology”) to obtain the relative resistance change (Fig. 2d–i and Fig. S3, ESI†). It can be seen that the waveform and amplitude of most letters are different, that is, they have their own characteristic information. In addition, the strain sensors were placed in a natural environment for more than two months to evaluate their efficacy in lip-reading signal extraction. The results indicated that the sensor had unique and repeatable peaks and valleys, regardless of whether the subjects read the letters or words “A”, “B”, “C” and “你好” in a stationary position (Fig. S4a–e, ESI†) or during walking dynamics (Fig. S4f–j, ESI†). These findings suggest that the strain sensor possesses commendable environmental stability,

repeatability, and interference resistance, rendering it suitable for a universal application in lip recognition.

In order to verify the important role of lip movement rather than vocalizing for lip-reading extraction and speech recognition, we tested the change of the electrical signal of the sensor when reading “A” and “D” with only lip movement without the vocal cord vibration (Fig. S5, ESI†). Compared with the relative electrical signal change of “A” and “D” in Fig. S3 (ESI†), their characteristic peaks are basically the same when the speaker does not pronounce and only changes his mouth shape. However, the detected electrical signals are entirely different in the cases of vocalization and non-vocalization when the sensor is attached to the vocal cords of the throat. This means that once the vocal cords are damaged, the muscle vibration in the throat cannot produce effective monitoring information. In addition, the electrical signal changes caused by the vibration of the vocal cords are much smaller than those produced by the muscles around the lips, indicating that the CuNW-rGO/PDMS composite strain sensor is a wise choice for lip language recognition, especially for dumb patients with acquired vocal cord damage.

Notice that some English letters, such as "A", "D", "K", "R" and "Y" present similar wave changes (Fig. S3, ESI<sup>†</sup>). To further distinguish these similar waveforms, the sensor is cut into an arc array with 5 detection units to better sense muscle movement of lip (Fig. 5a<sub>1</sub>), including the buccinator, depressor anguli oris, zygomaticus major, levator labii superioris, depressor labii inferioris, and levator anguli oris (Fig. 5a<sub>2</sub>). The electrical signal changes (amplitude and waveform) obtained from these 5 units cannot be exactly the same for several letters with similar signals. Therefore, the designed arc array can detect the differential deformation of the corresponding muscles at different positions of the lip, identifying similar waveforms of different letters and realizing flexible and efficient recognition.

In order to realize lip-reading recognition, we created a relatively simple and feasible lip-reading recognition system, including sensors, microcontroller systems (MCUs), hardware circuits and mobile phones. First, we collected lip-reading signals for common English and Chinese phrases (Fig. 6a) when the sensor was attached to the mouth corner, and 50 test signals were taken from each phrase to form a database of common lip-reading phrases (Fig. 6b). Then the signal was processed by an MCS (Fig. 6c). In the process of data analysis, we need to know the sizes of individual differences and then evaluate the individual similarity. To compare the differences between X and Y individuals, we mainly use distance measurement. Euclidean distance is the most common distance measurement, which measures the absolute distance between two points in multidimensional

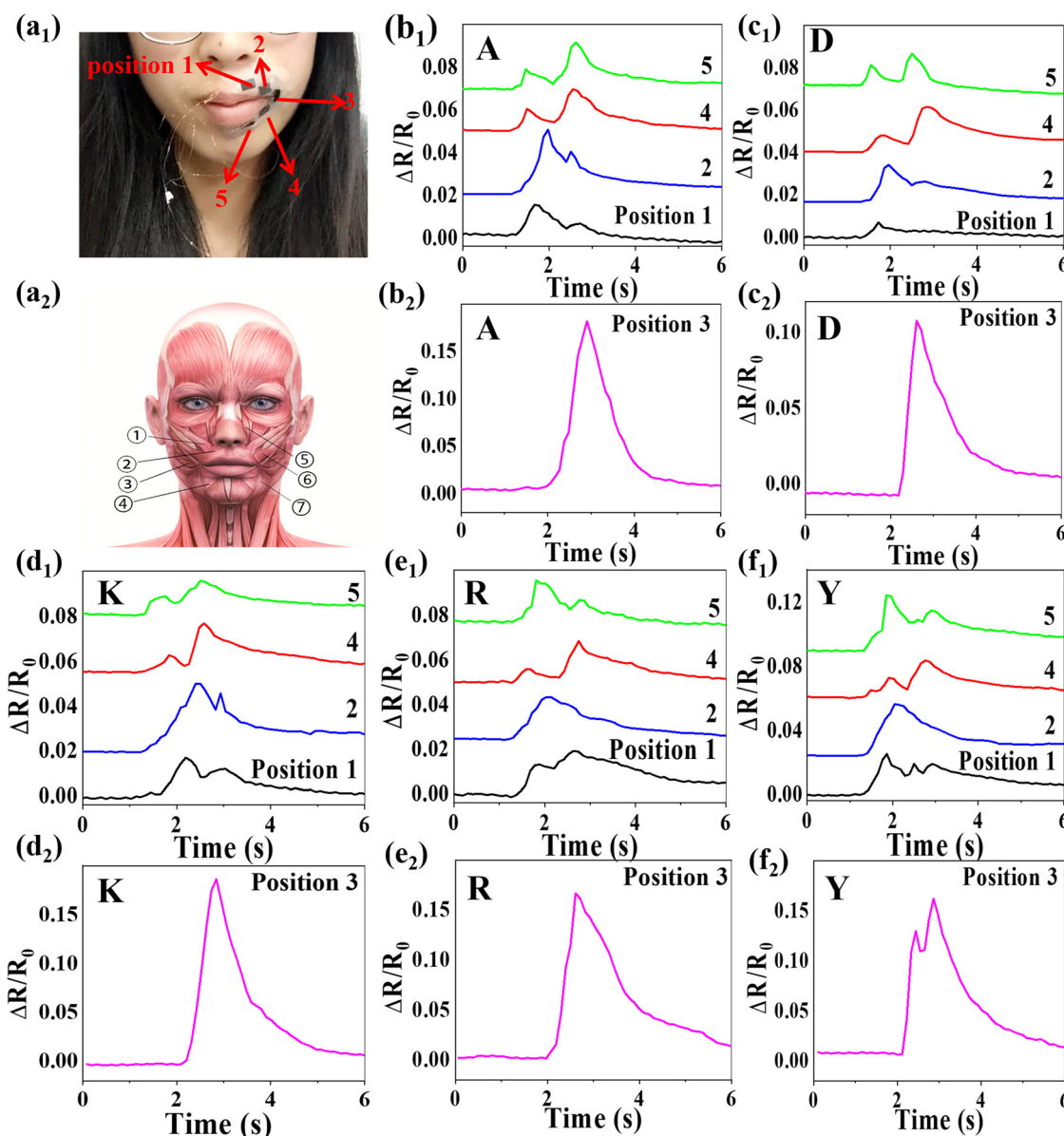


**Fig. 5** An arc array with 5 detection units is used to distinguish close waveforms of different letters. (a<sub>1</sub>) Photograph of location distribution of the arc array sensor. (a<sub>2</sub>) Lip muscle composition diagram: ① levator anguli oris, ② orbicularis oris muscle, ③ buccinator, ④ depressor labii inferioris, ⑤ levator labii superioris, ⑥ zygomaticus major, and depressor anguli oris. (b)–(f) Real-time tests of letters A, D, K, R, and Y at 5 different positions, respectively.

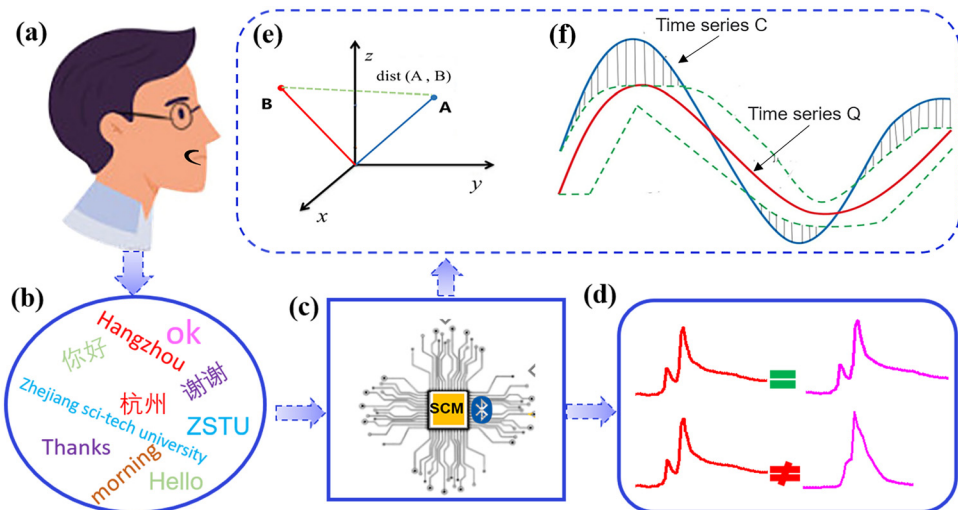


**Fig. 6** (a) Schematic diagram of a volunteer wearing a lip-reading sensor. (b) The database stores the collected lip reading signals. (c) MCS processes the collected signals for recognition. (d) Schematic diagram of matching and mismatching lip reading signal data. (e) and (f) are the schematic diagrams of Euclidean distance and DTW algorithms used by the MCU to process the lip reading signals.

space (Fig. 6e). The Euclidean distance between two  $n$ -dimensional vectors  $(x_{11}, x_{12}, \dots, x_{1n})$  and  $(x_{21}, x_{22}, \dots, x_{2n})$  is<sup>46</sup>

$$d = \sqrt{\sum_{k=1}^n (x_{1k} - x_{2k})^2}. \quad (1)$$

When the number of lip-reading signal sequences are different and cannot correspond to each other, we use the dynamic time warping (DTW) algorithm (Fig. 6f) to expand or reduce the sequences to the same number. By limiting the boundary conditions, continuity and monotonicity, the path

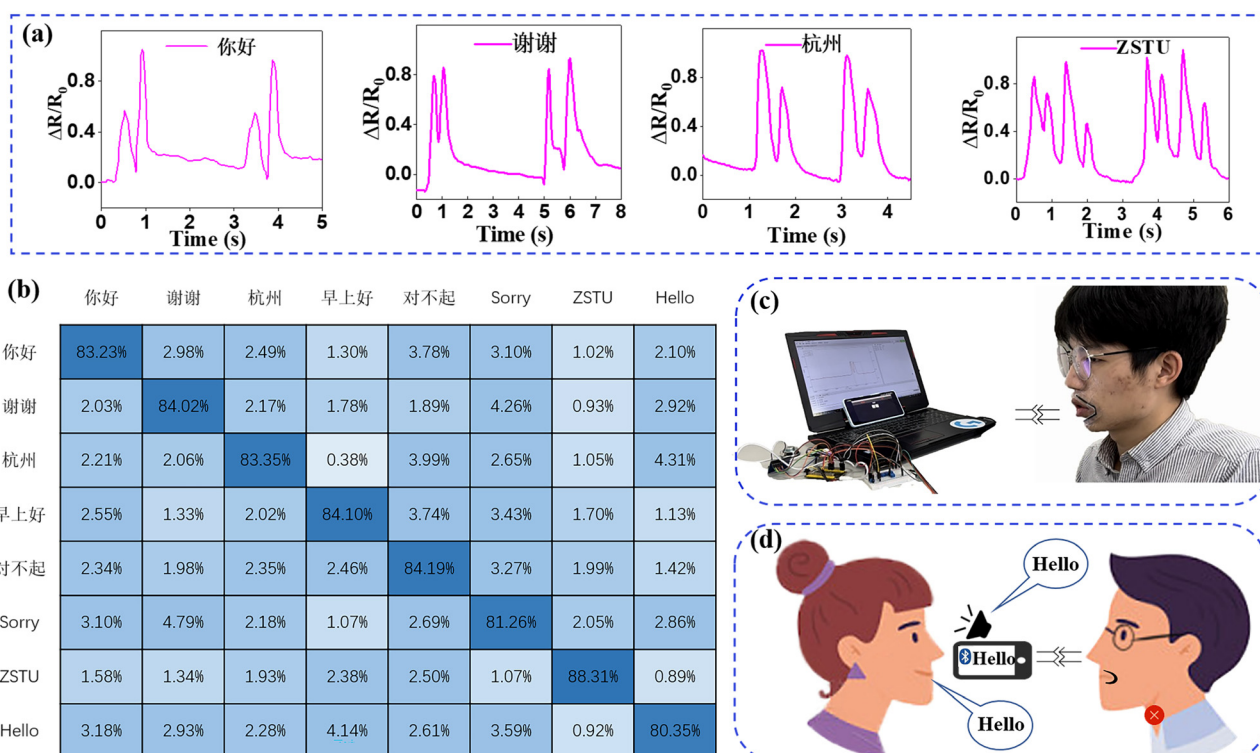


**Fig. 7** (a) The relative resistance changes of the sensor when reading some common Chinese and English phrases. (b) The recognition rate matrix of 8 phrases. (c) Optical image of a lip-reading recognition system with sensors worn by a volunteer. (d) Schematic illustration of a person with impaired vocal cords using a lip-reading recognition system to achieve barrier-free communication with normal people in speech and text.

with the least cost of regularization can be obtained<sup>47</sup>

$$\text{DTW}(Q, C) = \min \left( \sqrt{\sum_{k=1}^K w_k} \right) / K \quad (2)$$

here  $Q$  and  $C$  represent the time series of length  $n$  and  $m$ , respectively. The time warping path  $W$  consists of  $K$  elements. And  $w_k$  represents the  $k$ -th element of the time warping path, which is the Euclidean distance between the  $i$ -th element in sequence  $Q$  and the  $j$ -th element in sequence  $C$ ,  $w_k = d(Q_i, C_j)$ . Finally, we can use the minimum cumulative distances to represent the best path by using the algorithm<sup>48</sup>

$$\gamma(i, j) = d(Q_i, C_j) + \min\{\gamma(i - 1, j - 1), \gamma(i - 1, j), \gamma(i, j - 1)\} \quad (3)$$

here  $\gamma(i, j)$  represents the cumulative distances.

Take “你好”, “谢谢”, “Hangzhou”, “ZSTU”, “早上好”, “Sorry”, “对不起” and “Hello” as examples. Fig. 7a shows the different signal waveforms when the same person reads out different common Chinese and English phrases. After processing by the recognition algorithm of the microcontroller, the average recognition rate of common Chinese and English phrases is above 80% and most of the phrases can be accurately recognized (Fig. 7b). Furthermore, a communication module (Fig. 7c) was used to enable serial communication between the MCS and the Bluetooth module. The Bluetooth connects to the mobile phone and displays the recognized text information directly. A voice broadcast module outputs and plays the voice of the recognized lip language information (Fig. 7c). Video S1 (ESI†) shows a volunteer wearing sensors on his lips using a lip-reading recognition system in which voice and corresponding texts can be played and displayed from the mobile phone in real time. Additionally, consider the fact that patients with damaged vocal cords are unable to communicate with humans normally, our sensor can achieve barrier-free communication with normal people (Fig. 7d and Movie S2, ESI†) even when the user does not vocalize. This undoubtedly brings hope to the mute, especially those with acquired vocal cord damage, who only needs to wear lip-reading recognition and assisted pronunciation devices to achieve barrier-free communication with normal people.

## Conclusions

In conclusion, we proposed a simple and effective fabrication for a “brick-mortar” structure CuNW-rGO/PDMS hybrid film strain sensor using hydrothermal synthesis and filtration. The CuNW-rGO/PDMS composite porous film sensor exhibits excellent conductivity owing to the moderate addition of CuNWs and the improved sensitivity ( $GF = 26$ ) through different contact methods between the rGO sheet and CuNWs. The sensor can detect tensile strains over 70% and maintains excellent stability with more than 1000 loading-unloading cycles. Moreover, the strain sensor can be attached onto bodies to detect human body motions such as hand clenching, elbow bending and wrist pulse beating. Last but not least, the strain sensor, when attached

around lips, can be used for lip-reading signal acquisition, recognition and auxiliary pronunciation, helping individuals with speech impairments live a fulfilling life with accessible communication. This work also holds potential value in applications involving disability assistance, human-machine interfaces, silent speech, intelligence, anti-terrorism mission implementation and rehabilitation.

## Data availability

All data supporting the results are presented in the article, supplementary information and supplementary videos.

## Conflicts of interest

The authors declare that they have no conflicts of interest.

## Acknowledgements

This work was supported by the National Natural Science Foundation of China (No. 12272351, 11972323 and 11672269), the Youth Top-notch Talent Project of Zhejiang Ten Thousand Plan of China (No. ZJWR0308010), the Zhejiang Provincial Natural Science Foundation of China (No. LR20A020002, LQ20E010009 and LR19E020004), and the Zhejiang University Student Science and Technology Innovation Activity Plan (New Seedling Talent Plan) (2022R406A002).

## References

- 1 K. Noda, Y. Yamaguchi, K. Nakadai, H. G. Okuno and T. Ogata, *Appl. Intell.*, 2015, **42**, 722–737.
- 2 B. Yang and W. Yuan, *ACS Appl. Mater. Interfaces*, 2019, **11**, 40620–40628.
- 3 M. Swain, A. Routray and P. Kabisatpathy, *Int. J. Speech Technol.*, 2018, **21**, 93–120.
- 4 S. C. Lee, J. F. Wang and M. H. Chen, *Sensors*, 2018, **18**, 2068.
- 5 I. Ding Jr and C. M. Ruan, *J. Imaging Sci. Technol.*, 2019, **63**, 50402.
- 6 A. Brahme and U. Bhadade, *Int. J. Image Graph*, 2020, **20**, 2050029.
- 7 S. Jeon, A. Elsharkawy and M. S. Kim, *Sensors*, 2021, **22**, 72.
- 8 T. Sun, F. Tasnim, R. T. McIntosh, N. Amiri, D. Solav, M. T. Anbarani, D. Sadat, L. Zhang, Y. Gu, M. A. Karami and C. Dagdeviren, *Nat. Biomed. Eng.*, 2020, **4**, 954–972.
- 9 C. C. Wan, L. Y. Zhang, K. T. Yong, J. Li and Y. Q. Wu, *J. Mater. Chem. C*, 2021, **9**, 11001–11029.
- 10 J. A. Rogers, *Nat. Nanotechnol.*, 2017, **12**, 839–840.
- 11 J. Lee, B. L. Zambrano, J. Woo, K. Yoon and T. Lee, *Adv. Mater.*, 2020, **32**, 1902532.
- 12 K. K. Zhai, H. Wang, Q. L. Ding, Z. X. Wu, M. H. Ding, K. Tao, B. R. Yang, X. Xie, C. W. Li and J. Wu, *Adv. Sci.*, 2023, **10**, 2205632.

- 13 Z. Liu, T. Zhu, J. Wang, Z. Zheng, Y. Li, J. Li and Y. Lai, *Nano-Micro Lett.*, 2022, **14**, 1–39.
- 14 Z. X. Wu, H. Wang, Q. L. Ding, K. Tao, W. X. Shi, C. Liu, J. Chen and J. Wu, *Adv. Funct. Mater.*, 2023, 2300046.
- 15 X. H. Liu, J. L. Miao, Q. Fan, W. X. Zhang, X. W. Zuo, M. W. Tian, S. F. Zhu, X. J. Zhang and L. J. Qu, *Adv. Fiber Mater.*, 2022, **4**, 361–389.
- 16 J. Y. Li, Q. L. Ding, H. Wang, Z. X. Wu, X. C. Gui, C. W. Li, N. Hu, K. Tao and J. Wu, *Nano-Micro Lett.*, 2023, **15**, 105.
- 17 D. X. Lu, S. Q. Liao, Y. Chu, Y. B. Cai, Q. F. Wei, K. L. Chen and Q. Q. Wang, *Adv. Fiber Mater.*, 2023, **5**, 223–234.
- 18 S. H. Lin, L. T. Cao, Z. C. Lv, J. Ren and S. J. Ling, *Adv. Fiber Mater.*, 2022, **4**, 214–225.
- 19 G. F. Cai, J. X. Wang, K. Qian, J. W. Chen, S. H. Li and P. S. Lee, *Adv. Sci.*, 2017, **4**, 1600190.
- 20 L. Cheng, W. Qian, L. Wei, H. J. Zhang, T. Y. Zhao, M. Li, A. P. Liu and H. P. Wu, *J. Mater. Chem. C*, 2020, **8**, 11525–11531.
- 21 W. Zhai, J. Zhu, Z. Wang, Y. Zhao, P. Zhan, S. Wang, G. Zheng, C. Shao, K. Dai, C. Liu and C. Shen, *ACS Appl. Mater. Interfaces*, 2022, **14**, 4562–4570.
- 22 X. Fang, J. Tan, Y. Gao, Y. Lu and F. Xuan, *Nanoscale*, 2017, **9**, 17948–17956.
- 23 J. K. Huang, J. B. Zeng, B. Q. Liang, J. W. Wu, T. G. Li, Q. Li, F. Feng, Q. W. Feng, M. J. Rood and Z. F. Yan, *ACS Appl. Mater. Interfaces*, 2020, **12**, 16822–16830.
- 24 L. Q. Tao, H. Tian, Y. Liu, Z. Y. Ju, Y. Pang, Y. Q. Chen and T. L. Ren, *Nat. Commun.*, 2017, **8**, 1–8.
- 25 J. Wang, L. Liu, C. Yang, C. Zhang, B. Li, X. Meng and L. Ren, *ACS Appl. Mater. Interfaces*, 2022, **14**, 16885–16893.
- 26 Y. Lu, H. Tian, J. Cheng, F. Zhu, B. Liu, S. Wei and Z. L. Wang, *Nat. Commun.*, 2022, **13**, 1–12.
- 27 J. Wu, W. X. Huang, Z. X. Wu, X. Yang, A. G. P. Kottapalli, X. Xie, Y. B. Zhou and K. Tao, *ACS Mater. Lett.*, 2022, **4**, 1616–1629.
- 28 X. Y. Meng, S. F. Zhao, Z. Zhang, R. L. Zhang, J. H. Li, J. F. Leng, D. X. Cao, G. P. Zhang and R. Sun, *J. Mater. Chem. C*, 2019, **7**, 7061–7072.
- 29 X. L. Shi, H. K. Wang, X. T. Xie, Q. W. Xue, J. Y. Zhang, S. Q. Kang, C. H. Wang, J. J. Liang and Y. S. Chen, *ACS Nano*, 2019, **13**, 649–659.
- 30 Y. Huang, X. Y. You, Z. Q. Tang, K. Y. Tong, P. Guo and N. Zhao, *Small Methods*, 2021, 2000842.
- 31 N. Q. Luo, Y. Huang, J. Liu, S. C. Chen, C. P. Wong and N. Zhao, *Adv. Mater.*, 2017, **29**, 1702675.
- 32 Z. L. Tian, Y. Zhao, S. G. Wang, G. D. Zhou, N. Zhao and C. P. Wong, *J. Mater. Chem. A*, 2020, **8**, 1724–1730.
- 33 Y. P. Yang, Y. F. Sun, C. Z. Luo, Q. Fu and C. X. Pan, *Sens. Actuators, A*, 2021, **327**, 112754.
- 34 Q. Liu, M. Zhang, L. Huang, Y. Li, J. Chen, C. Li and G. Shi, *ACS Nano*, 2015, **9**, 12320–12326.
- 35 K. N. Kudin, B. Ozbas, H. C. Schniepp, R. K. Prud'Homme, I. A. Aksay and R. Car, *Nano Lett.*, 2008, **8**, 36–41.
- 36 X. Xiao, L. Yuan, J. Zhong, T. Ding, Y. Liu, Z. Cai, Y. G. Rong, H. W. Han, J. Zhou and Z. L. Wang, *Adv. Mater.*, 2011, **23**, 5440–5444.
- 37 X. Wang, L. Dong, H. Zhang, R. Yu, C. Pan and Z. L. Wang, *Adv. Sci.*, 2015, **2**, 1500169.
- 38 Y. Xiong, Y. Zhu, X. Liu, P. Zhu, Y. Hu, R. Sun and C. P. Wong, *Mater. Today Commun.*, 2020, **24**, 100970.
- 39 Y. R. Jeong, H. Park, S. W. Jin, S. Y. Hong, S. S. Lee and J. S. Ha, *Adv. Funct. Mater.*, 2015, **25**, 4228–4236.
- 40 M. Elpeltagy, M. Abdelwahab, M. E. Hussein, A. Shoukry, A. Shoala and M. Galal, *IET Comput. Vis.*, 2018, **12**, 1031–1039.
- 41 A. Venugopalan and R. Reghunadhan, *Expert Syst. Appl.*, 2021, **185**, 115601.
- 42 Y. Lu and H. Li, *Appl. Sci.*, 2019, **9**, 1599.
- 43 P. Kumar, P. P. Roy and D. P. Dogra, *Inf. Sci.*, 2018, **428**, 30–48.
- 44 S. Timilsina, H. G. Shin, K.-S. Sohn and J. S. Kim, *Adv. Intell. Syst.*, 2021, **4**, 2000036.
- 45 S. Ye, A. R. Rathmell, I. E. Stewart, Y. C. Ha, A. R. Wilson, Z. Chen and B. J. Wiley, *Chem. Commun.*, 2014, **50**, 2562–2564.
- 46 P. Breiding, F. Sottile and J. Woodcock, *Found. Comput. Math.*, 2022, **22**, 1743–1765.
- 47 Y. Y. Zhang, Y. Huang, X. H. Sun, Y. N. Zhao, X. H. Guo, P. Liu, C. X. Liu and Y. G. Zhang, *IEEE Sens. J.*, 2020, **20**, 6450–6459.
- 48 H. L. Li and C. Wang, *IEEE Access*, 2018, **7**, 3909–3917.